Self-Coherent Camera: active correction and post-processing for Earth-like planet detection

Raphaël Galicher[a] Pierre Baudoz[a] Gérard Rousset[a]

[a] LESIA, CNRS, Observatoire de Paris, 5, place Jules Janssen, 92195 Meudon, France*

ABSTRACT

Detecting light from faint companions or protoplanetary disks lying close to their host star is a demanding task since these objects are often hidden in the overwhelming star light. A lot of coronagraphs have been proposed to reduce that stellar light and thus, achieve very high contrast imaging, which would enable to take spectra of the faint objects and characterize them. However, coronagraph performance is limited by residual wavefront errors of the incoming beam which create residual speckles in the focal plane image of the central star. Correction or calibration of the wavefront are then necessary to overcome that limitation. We propose to use a Self-Coherent Camera (SCC, Baudoz et al. 2006). The SCC is one of the techniques proposed for EPICS, the futur planet finder of the European Extremely Large Telescope but can also be studied in a space telescope context. The instrument is based on the incoherence between stellar and companion lights. It works in two steps. We first estimate wavefront errors to be corrected by a deformable mirror and then, we apply a post-processing algorithm to achieve very high contrast imaging.

Keywords: Instrumentation, High contrast imaging, High angular resolution, exoplanet, wavefront correction, dark hole

1. INTRODUCTION

Only indirect detections were available in 1995 when Mayor&Quéloz [1] have discovered the first extrasolar planet. Since one of the most expected results is to evaluate the habitability of exoplanets, indirect detections were not sufficient and forces have been put on direct detection technique development. The first difficulty of such techniques is the exoplanet incoming light flux is very faint compared to its host star: 10^7 and 10^{10} fainter respectively for a Jupiter and an Earth-like planet in visible wavelength. That is why we first need to reduce the stellar flux without reducing the exoplanet one. In that way, numerous coronagraphs have been proposed, studied and built. Great results have been demonstrated by simulation[2] and laboratory experiment.[3] However, all coronagraphs are limited by the uptream wavefront aberrations so that the coronagraphic image is dominated by residual stellar speckles and companions are not detected. Adaptive optics have requiered to correct most of these aberrations. Some remain uncorrected generating quasi-static residual speckles.[4] To calibrate them, Baba et al.[5] or Marois et al.[6] have suggested to substract a reference image (without companions) to the science image (with companions) using spectral or polarization characteristics of the companions. Other techniques which do not depend on specific companion characteristics are based on the incoherence between the lights incoming from the star and the companion. A Reference wavefront composed only by stellar light is created from the rejected light by the coronagraph. Then, that Reference channel is recombined with the coronagraphic residu to make them interfer. As long as companion and stellar light are not coherent, only stellar lights from the two channels can interfer. As a consequence, comparing to the coronagraphic image, companion images are unchanged while residual stellar speckles are temporally[7] or spatially[8] encoded and thus calibrated. Such a technique, the Self-Coherent Camera (SCC), has been proposed by Baudoz et al..[9] The calibration given by the SCC can be used to suppress the calibrated residual speckles in a post-processed treatment.[10] An other way is to estimate, from the calibration, the wavefront errors in order to correct them by an upstream deformable mirror.[11] In the first section of that paper, we briefly describe the SCC principle. Then, we derive the estimator of wavefront aberrations for polychromatic light in section 3. In section 4, we explain the post-processing algorithm in polychromatic light. Section 5 presents SCC performances under realistic assumtions for a space telescope.

*Groupement d'Intérêt Scientifique PHASE (Partenariat Haute résolution Angulaire Sol Espace) between ONERA, Observatoire de Paris, CNRS and University Denis Diderot Paris 7.

E-mail: raphael.galicher@obspm.fr, Phone number: +33 (0)1 45 07 75 12

2. SCC PRINCIPLE

The principle of the Self-Coherent Camera has already been detailed in previous papers.[9,10] Here, we recall the main part of the technique. The beam incoming from the telescope is reflected on a deformable mirror (DM) and is splitted into two channels (figure 1). The Image channel (red in electronic edition) propagates through

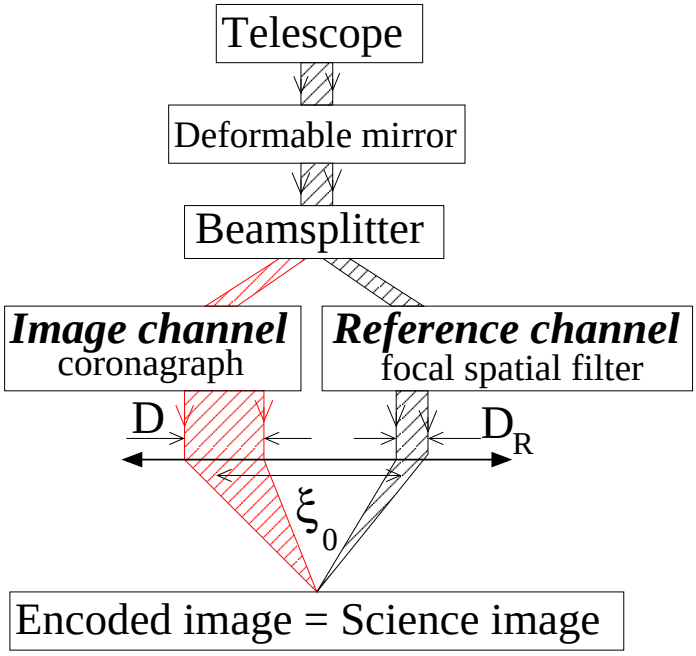

Figure 1. *Self-Coherent Camera principle schema.*

a coronagraph. It contains companion light and residual stellar light due to upstream wavefront errors. We call $\Psi_{\rm S}(\xi) + \Psi_{\rm C}(\xi)$ its complex amplitude, where ξ is the pupil coordinate. $\Psi_{\rm S}$ and $\Psi_{\rm C}$ respectively represent stellar and companion complex amplitudes of the field in the pupil plane just after the D diameter Lyot stop. The second channel, called Reference channel, is spatially filtered in a focal plane using a pinhole which radius is smaller than λ/D. Almost all the companion light is stopped since it is not centered on the pinhole. In the pupil plane just after the $D_{\rm R}$ diameter diaphragm we name $\Psi_{\rm R}(\xi)$ the Reference complex amplitude. The pinhole reduces impact of wavefront errors on $\Psi_{\rm R}$ since it acts as a spatial frequency filter. An optic recombines the two channels, separated by ξ_0 in the pupil plane, and creates a Fizeau fringed pattern in a focal plane. We can notice the SCC differs from Codona's and Guyon's techniques where channels are recombined on axis as in a Michelson scheme. In the SCC, residual speckles are thus spatially encoded unlike companions. The mean intensity of residual speckles of the Image channel is almost spatially constant and very attenuated because of the coronagraph. To optimize fringe contrast, we have to match intensity distributions and fluxes of Image and Reference channels. We use a $D_{\rm R} < D$ diameter diaphragm to obtain an almost flat Reference intensity in the focal plane. We can notice that diaphragm reduces again the impact of aberrations on $\Psi_{\rm R}$ since only a few $\lambda/D_{\rm R}$ are visible in the image. Thus, the Reference channel is not very sensitive to aberrations and can be calibrated before the interference recording.[10] Fluxes are equalized using a variable neutral density in the Reference channel before the pinhole (section 5). In figure 2, we present, at the same spatial scale, (a) the image formed after the sole coronagraph for the pupil of diameter D (sole Image channel) showing residual speckles, (b) the image corresponding to the sole Reference channel for the pupil of diameter D_R and (c) the interferential image where the residual speckles are spatially encoded by fringes.

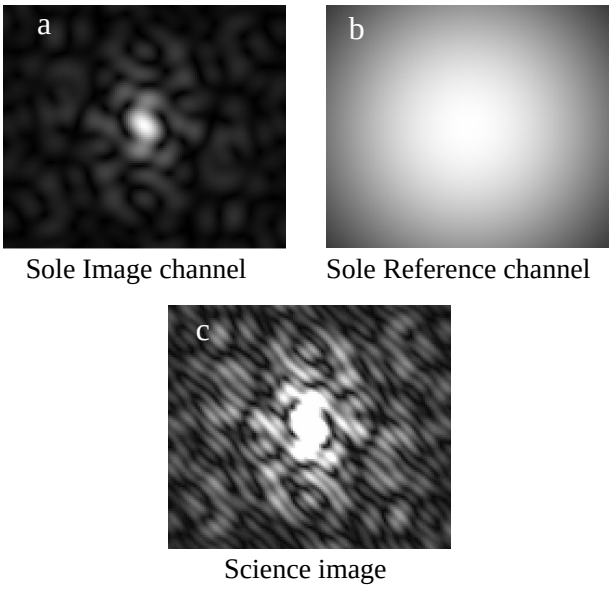

Figure 2. *(a) Image formed after the sole coronagraph for the pupil of diameter D (sole Image channel) showing the residual speckles. (b) Image of the sole Reference channel for the pupil of diameter D_R. (c) Interferential image (science image) where the speckles are spatially encoded by fringes. The spatial scale is the same for all the images.*

In polychromatic light, the intensity $I(\alpha)$ in the last focal plane is

$$I(\alpha) = \int_{\mathcal{R}} \frac{1}{\lambda^2} \left[I_{\mathrm{S}} \left(\frac{\alpha\, D}{\lambda} \right) + I_{\mathrm{R}} \left(\frac{\alpha\, D}{\lambda} \right) + I_{\mathrm{C}} \left(\frac{\alpha\, D}{\lambda} \right) + 2\, Re \left(A_{\mathrm{S}} \left(\frac{\alpha\, D}{\lambda} \right) A_{\mathrm{R}}^{*} \left(\frac{\alpha\, D}{\lambda} \right) \exp \left(\frac{2\, i\, \pi\, \alpha\, \xi_0}{\lambda} \right) \right) \right] d\lambda \tag{1}$$

where α is the angular coordinate in the image, A_i the Fourier tranform of the corresponding Ψ_i, I_i the intensity $|A_i|^2$ and A_i^* the conjugate of A_i. The wavelength λ belongs to $\mathcal{R} = [\lambda_0 - \Delta\lambda/2, \lambda_0 + \Delta\lambda/2]$. We can use that image (figure 3), recorded on the detector, in two ways. First, we can estimate the upstream wavefront aberrations and drive a deformable mirror to correct them as described in section 3. An other possibility is to apply a post-processing algorithm[9,10] to suppress the fringed and thus, encoded speckles as we explain quickly in section 4.

3. WAVEFRONT ABERRATION ESTIMATION

Following first work by Bordé&Traub,[12] we want to estimate wavefront errors from residual speckles (equation 1). For this purpose, we propose to extract the modulated part of I which contains a linear combination of A_{S} and A_{R}. First, we apply a Fourier Transform on I. We isolate one of the lateral correlation peaks, apply an inverse Fourier Transform and obtain I_{-}.

$$I_{-}(\alpha) = \int_{\mathcal{R}} \frac{1}{\lambda^2} A_{\mathrm{S}} \left(\frac{\alpha\, D}{\lambda} \right) A_{\mathrm{R}}^{*} \left(\frac{\alpha\, D}{\lambda} \right) \exp \left(\frac{2\, i\, \pi\, \alpha\, \xi_0}{\lambda} \right) d\lambda \tag{2}$$

In equation 2, A_{S} and A_{R}^{*} depend on $\alpha D/\lambda$, inducing the speckle dispersion with wavelength. Fizeau interfringe λ/ξ_0 is proportional to wavelength in the exponential term. Both effects degrade the wavefront estimation from I_{-} when useful bandwidth is large but the wavelength fringe dependence is dominant. We may want working with an Integral Field Spectrometer at modest resolution ($R = 100$) or faking the use of short bandpass filter with a chromatic compensator. Such a device proposed by Wynne[13] almost compensates the two chromatic effects over a large spectral band ($\Delta\lambda \simeq 0.2\, \lambda_0$) to give a smaller effective bandwidth ($\Delta\lambda_{\mathrm{eff}} \simeq 0.01\, \lambda_0$). It allows

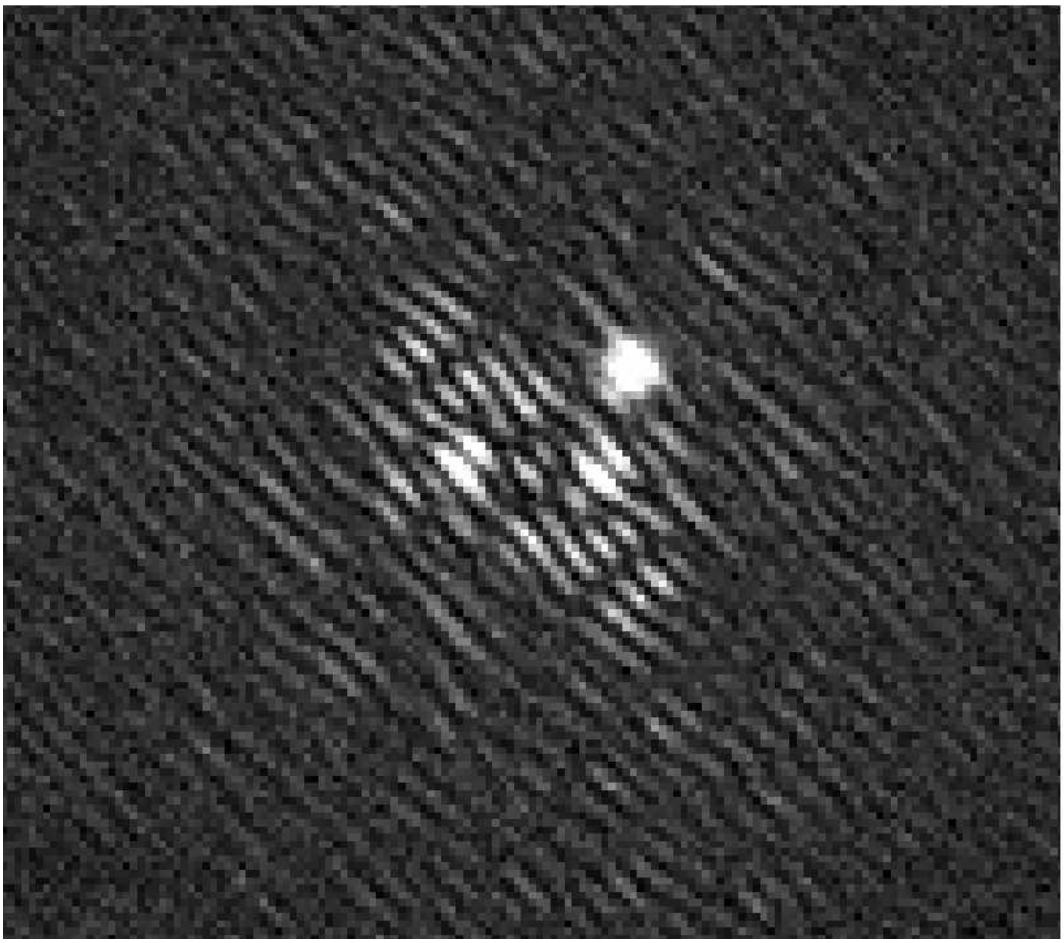

Figure 3. *SCC interferential image. Residual speckles are fringed while companion image is not. To show that difference, contrast between companion and star has been set to* 1 *since it is about* 10^{-7} *to* 10^{-10} *in reality.*

us to be close to a monochromatic case in our model of SCC image formation. We firstly assume $\Delta\lambda_{\text{eff}} \ll \lambda_0$ so that A_{S} and A^*_{R} are constant over the spectral band. We obtain from equation 2

$$I_-(\alpha) \simeq A_{\text{S}}\left(\frac{\alpha\, D}{\lambda_0}\right) A^*_{\text{R}}\left(\frac{\alpha\, D}{\lambda_0}\right) \int_{\mathcal{R}} \frac{1}{\lambda^2} \exp\left(\frac{2\, i\, \pi\, \alpha\, \xi_0}{\lambda}\right) d\lambda \tag{3}$$

The term to estimate is A_{S} and more precisely, its inverse Fourier transform Ψ_{S}. We deduce from equation 3

$$\Psi_{\text{S}}(\xi) \simeq \mathcal{F}^{-1}\left[\frac{I_-(\alpha)\, F^*(\alpha)}{A^*_{\text{R}}(\alpha D/\lambda_0)\, \|F\|^2}\right] \tag{4}$$

where $\mathcal{F}^{-1}$ denotes the inverse Fourier transform, F represents $\displaystyle\int_{\mathcal{R}} \frac{1}{\lambda^2} \exp\left(2\, i\, \pi\, \alpha\, \xi_0/\lambda\right) d\lambda$ and F^* its conjugate. As a second assumption, we consider wavefront errors ϕ we are searching for are small and we can write the star field Ψ'_{S} in the pupil plane upstream the coronagraph

$$\Psi'_{\text{S}}(\xi) \simeq \Psi_0\, P(\xi) \left(1 + \frac{2\, i\, \pi\, \phi(\xi)}{\lambda_0}\right) \tag{5}$$

where Ψ_0 is the amplitude of the star assumed to be uniform over P, the unitary flat pupil of diameter D. In a third step, we assume a perfect achromatic coronagraph ,[4] which allows us to remove the coherent part of

energy $\Psi_0\,P$ to $\Psi'_{\rm S}$

$$\Psi_{\rm S}(\xi) \simeq \frac{2\,i\,\pi}{\lambda_0}\,\Psi_0\,P(\xi)\,\phi(\xi) \tag{6}$$

Finally, equation 4 and 6 give an estimator of wavefront errors within the pupil

$$\phi(\xi) \simeq \frac{\lambda_0}{2\,\pi}\left[\mathcal{I}\left\{\mathcal{F}^{-1}\left[\frac{I_-(\alpha)\,F^*(\alpha)}{\Psi_0\,A^*_{\rm R}(\alpha D/\lambda_0)\,\|F\|^2}\right]\right\}\right] \tag{7}$$

with $\mathcal{I}\{\,\}$ the imaginary part. In equation 7, F depends only on known physical parameters, ξ_0 and the spectral bandwidth, and is numerically evaluated. We can estimate Ψ_0 since we can calibrate the incoming flux star collected by the telescope. I_- is derived from the recorded image I. Finally, we have to divide by the complex amplitude $A^*_{\rm R}$, previously calibrated (section 2). Setting $D_{\rm R} << D$, we obtain an almost flat Reference intensity and thus avoid values close to zero in the numeric division. Once wavefront errors are estimated from equation 7, we drive the DM to compensate them. Then, we record a new interferential image where quasi-static residual speckles have been suppressed and where companions are now detectable. Pratically, as we made assumptions to derive the estimator and because of noises, few iterations are required to reach high contrasts as shown in section 5. Once the best DM correction is achieved, we propose to improve the image contrast by applying a post-processing imaging that we describe in section 4.

4. POST-PROCESSING ALGORITHM

In that section, we quickly recall the principle of the post-processing algorithm we have already proposed in previous papers.[9,10] In figure 3, the companion is visible, and thus detected, because the contrast with its hosting star has been set to 1. This was done to show the companion image is not fringed unlike the star one. However, the contrast for an Earth-Sun system is about 10^{-10} in visible light. In that case, the companion is not detected on the interferential image and a second step in the SCC technique is needed : the extraction of the companion information from the interferential image. The current algorithm we use begins applying a Fourier tranform on the encoded image (cf. equation 1). We obtain three autocorrelation peaks. All the companion information is contained into the central peak while all the stellar speckle information is encoded into the two lateral peaks. Separating the three peaks and applying reverse Fourier transform, we obtain three variables in polychromatic light :

$$\left\{\begin{array}{l} I_1(\alpha) = \displaystyle\int_{\mathcal{R}}\left[I_{\rm S}\left(\frac{\alpha D}{\lambda}\right) + I_{\rm C}\left(\frac{\alpha D}{\lambda}\right) + I_{\rm R}\left(\frac{\alpha D}{\lambda}\right)\right]\,d\lambda \\ I_+(\alpha) = \displaystyle\int_{\mathcal{R}}\left[A^*_{\rm S}\left(\frac{\alpha D}{\lambda}\right)\,A_{\rm R}\left(\frac{\alpha D}{\lambda}\right)\exp\left(-\frac{2\pi\,\alpha\,\xi_0}{\lambda}\right)\right]\,d\lambda \\ I_-(\alpha) = \displaystyle\int_{\mathcal{R}}\left[A_{\rm S}\left(\frac{\alpha D}{\lambda}\right)\,A^*_{\rm R}\left(\frac{\alpha D}{\lambda}\right)\exp\left(\frac{2\pi\,\alpha\,\xi_0}{\lambda}\right)\right]\,d\lambda \end{array}\right. \tag{8}$$

By using the first assumption ($\Delta\lambda_{\rm eff} \ll \lambda_0$) of section 3, we deduce

$$\left\{\begin{array}{l} I_1(\alpha) \simeq I_{\rm S}\left(\frac{\alpha D}{\lambda_0}\right) + I_{\rm C}\left(\frac{\alpha D}{\lambda_0}\right) + I_{\rm R}\left(\frac{\alpha D}{\lambda_0}\right) \\ I_+(\alpha) \simeq A^*_{\rm S}\left(\frac{\alpha D}{\lambda_0}\right)\,A_{\rm R}\left(\frac{\alpha D}{\lambda_0}\right)\,F^*(\alpha) \\ I_-(\alpha) \simeq A_{\rm S}\left(\frac{\alpha D}{\lambda_0}\right)\,A^*_{\rm R}\left(\frac{\alpha D}{\lambda_0}\right)\,F(\alpha) \end{array}\right. \tag{9}$$

The two lateral peaks are used to estimate the star image because

$$I_{\mathrm{S}}\left(\frac{\alpha D}{\lambda_0}\right) = \frac{I_+(\alpha\, D/\lambda_0)\, I_-(\alpha\, D/\lambda_0)}{I_{\mathrm{R}}(\alpha\, D/\lambda_0)\, \|F\|^2} \tag{10}$$

and then, we deduce the companion intensity I_{C}

$$I_{\mathrm{C}}\left(\frac{\alpha D}{\lambda_0}\right) = I_1\left(\frac{\alpha D}{\lambda_0}\right) - I_{\mathrm{R}}\left(\frac{\alpha D}{\lambda_0}\right) - \frac{I_+(\alpha\, D/\lambda_0)\, I_-(\alpha\, D/\lambda_0)}{I_{\mathrm{R}}(\alpha\, D/\lambda_0)\, \|F\|^2} \tag{11}$$

Equation 11 gives the companion image as far as we have recorded the Reference image I_{R}. This can be done because the Reference channel is not very sensitive to aberrations and can be very stable in time (see section 2). In future paper, we will study the exact impact of variations of the aberrations on the SCC performances. Assuming we record $\overline{I_{\mathrm{R}}}$, which is an estimate of I_{R}, the star estimator $I_{\mathrm{S\,est}}$ and the companion image estimator, called I_{est}, are given by:

$$\begin{cases} I_{\mathrm{S\,est}}\left(\dfrac{\alpha D}{\lambda_0}\right) = \dfrac{I_+(\alpha\, D/\lambda_0)\, I_-(\alpha\, D/\lambda_0)}{\overline{I}_{\mathrm{R}}(\alpha\, D/\lambda_0)\, \|F\|^2} & (12) \\ I_{\mathrm{est}}\left(\dfrac{\alpha D}{\lambda_0}\right) = I_1\left(\dfrac{\alpha D}{\lambda_0}\right) - I_R\left(\dfrac{\alpha D}{\lambda_0}\right) - \dfrac{I_+(\alpha\, D/\lambda_0)\, I_-(\alpha\, D/\lambda_0)}{\overline{I_{\mathrm{R}}}(\alpha\, D/\lambda_0)\, \|F\|^2} & (13) \end{cases}$$

These estimators are valid for an exposure for the interferential image shorter than the coherent time of speckles [9] and for $\Delta\lambda_{\mathrm{eff}} \ll \lambda_0$. Equation 13 is true for any aberration or illumination of I_{S} or I_{R}. Thus, neither the non-uniform illumination of I_{R} because of spatial filtering nor any differential static aberration between the Reference and the Image channels limit the detection of a companion with the SCC.[10] However, the recorded image $\overline{I}_{\mathrm{R}}$ used in equation 13, is not exactly the same as the image I_{R} of the real expression of I_{C} (equation 11). In first order, only the energy levels differ and we can optimize the level of $\overline{I}_{\mathrm{R}}$ in equation 13. The second point is the presence of pixels with a very low value in $\overline{I}_{\mathrm{R}}$. Indeed, estimating I_{*est} using equation 12, computers give very high values for these pixels and then amplify the noise on low intensity pixels. However, as shown in figure 2, the Reference image I_{R} is spatially very large because of the small diameter of the diaphragm $D_R \ll D$. This avoids the low value pixels. We do not detail results achieved by the SCC post-processing algorithm since they are available in previous papers.[9, 10]

To sum up sections 3 and 4, we propose to use the Self-Coherence Camera in two steps. First, we estimate wavefront aberrations from the Science image and drive a deformable mirror to correct them. Once the best correction is achieved, we apply the post-processing algorithm to detect the companions.

5. PERFORMANCES

In that section, we consider SCC device working at visible light ($\lambda_0 = 0.8\,\mu m$, $\Delta\lambda \simeq 0.2\,\lambda_0$, $\Delta\lambda_{\mathrm{eff}} = 0.01\,\lambda_0$, section 2). We suppose a perfect achromatic coronagraph. The beamsplitter injects 99% of the incoming energy in the Image channel. The filtering pinhole radius is λ_0/D and $D = 25\,D_{\mathrm{R}}$. To be more realistic, we assume a calibration of the Reference channel with a non-aberrated incoming wavefront and use it in the estimator of equation 7. To not overlap autocorrelation peaks of $\mathcal{F}(I)$, we choose $\xi_0 = 1.05\,(1.5\,D + 0.5\,D_{\mathrm{R}})$. We use 1024×1024 pixel interferential images with 4 pixels for the smallest interfringe over $\mathcal{R}$. We consider static aberrations in the instrument upstream of the coronagraph. We adopt a 20 nm rms amplitude with a spectral power density varying as f^{-3}, where f is the spatial frequency, which corresponds to the VLT optic aberrations.[12] We assume a 32×32 DM. The nth-actuator influence function is $\exp\left(-1.22\,(32\,(\xi - \xi_{\mathrm{n}})/D)^2\right)$, where ξ_{n} is the center of the nth-actuator. We call $\mathcal{H}$ the $(32\,\lambda_0/D)^2$ corrected area which is centered on-axis. We simulate an 8 m-diameter space telescope with a 50% throughput and pointing a G2 star at 10 parsec. The quantum efficiency of the detector is 50%. We consider photon noise, set the read-out-noise to $5e-$ per pixel and take into consideration zodiacal light as a uniform background at 22.5 mag.arcsec^{-2}.

Correcting wavefront errors, we improve the coronographic rejection and Reference intensity $I_{\rm R}$ becomes dominant in the science image I (equation 1). We adjust a calibrated neutral density in the Reference channel at each step. We estimate the ratio r of incoming energies from Image and Reference channels in the center of the image – $r = \int_{\mathcal{H}'} (I(\alpha) - I_{\rm R}(\alpha)) / \int_{\mathcal{H}'} I_{\rm R}(\alpha)$ with $\mathcal{H}'$ the $(22\lambda_0/D)^2$ centered on-axis area – and optimize fringe contrast for the next step. Finally, intensity in $\mathcal{H}$ decreases as the coronagraphic rejection increases. At each step, we adjust the exposure time to optimize the signal to noise ratio in the 16-bit dynamic range of the detector.

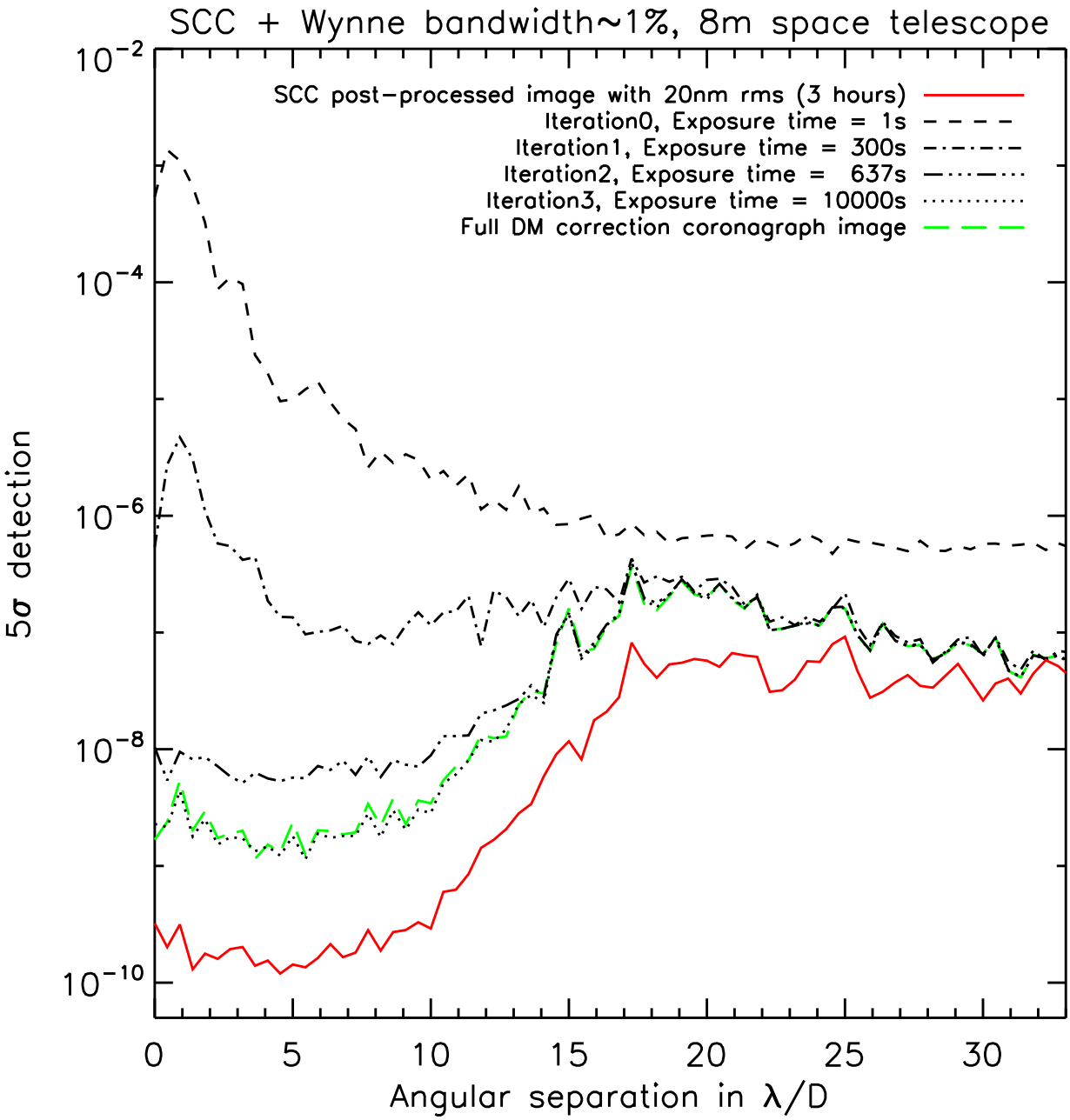

Figure 4. *5σ detection limit vs angular separation.*

We plot in figure 4 the 5σ detection limit of the interferential image I versus angular separation for several

iterations of the correction. The 5σ detection limit corresponds to an azimuthal average.[4] We specify in the figure the exposure time of each step. Iteration 0 gives the coronagraphic residue due to the 20 nm rms static aberrations without any correction. The algorithm of section 3 converges in a few steps (~ 3). Dashed green line represents the coronagraphic image, without SCC, computed with a full correction by the 32×32 DM. That curve is almost surperimposed to the curve of iteration 3. This shows the SCC achieves the detection floor due to uncorrectable high order aberrations. The level of that limit depends only on the number of actuators of the DM and the initial aberration level.[12] To improve the performance, we may increase the number of DM actuators or work with better optics. In a second step, we apply on the last iteration image the post-processing algorithm of section 4. The 5σ detection limit of the SCC post-processed image is plotted in figure 4 (red full line). The gain in $5\,\sigma$ detection is about 10^5 at $5\,\lambda_0/D$ in a few steps. An Earth-like planet, 2.10^{-10} fainter than its host star, is detected at $5\,\sigma$ in about 3 hours. Contrast outside $\mathcal{H}$ is slightly improved during first steps because the Reference flux decreases (neutral density) and the corresponding noise also.

Under the same assumptions, we simulate four $2\,10^{-10}$ companions respectively at 1, 3, 5 and $7\,\lambda_0/D$ (0.02, 0.06, 0.10 and 0.14 arcsec) including their photon noise. As shown in figure 5, these Earth-like planets are detected in the SCC post-processed image after a total exposure time T of ~ 3 hours. The accuracy on measured positions is a fraction of λ/D (less than $\lambda/(2\,D)$). Fluxes are determined within a 20% precision for the three most off-axis companions. Coronagraph degrades the accuracy on the measured flux of the closest one ($1\,\lambda_0/D$). The efficiency of the post-processing algorithm should be improved in future studies. We can notice that the correction area is larger in the fringe direction (from top-left to bottom-right) because of the residual chromatic dispersion effect (equation 2).

Similar results of very high contrast imaging have been demonstrated by Trauger&Traub[3] in a laboratory experiment. They have achieved a very high contrast of 10^{-9} in polychromatic light ($\Delta\lambda \simeq 0.02\,\lambda_0$), corresponding to a $5\,\sigma$ detection of 5.10^{-9}.

6. CONCLUSIONS

We have numerically demonstrated that the SCC associated with a 32×32 DM enables to detect Earths from space in a few hours when using realistic assumptions (zodiacal light, photon noise, read-out-noise, VLT pupil aberrations, 20% bandwidth). SCC could be a good candidate to be implemented in the next generation of space telescopes. The technique requires two steps. We first use SCC to estimate wavefront errors and drive a DM which correction limitation is reached in a few steps. We then overcome that usual limitation by applying, on the last iteration image, the SCC post-proccessing algorithm. This post-processing has still to be improved.

SCC is one of the techniques under investigation for the E-ELT planet finder so-called EPICS. In this context, we will consider impact of different parameters such as amplitude errors and turbulence residuals on the SCC performance. We will also test the compensation for amplitude errors as proposed by Bordé&Trauub.[12] The quality of Reference beam should not be critical for SCC because of the filtering by the pinhole and the reduction of the beam diameter (D_R) inducing a large diffraction pattern in the focal plane. Experimental validations of the SCC technique are also planned soon.

REFERENCES

1. Mayor, M. and Queloz, D., "A Jupiter-Mass Companion to a Solar-Type Star," *Nature* **378**, 355–+ (Nov. 1995).
2. Guyon, O., Pluzhnik, E. A., Kuchner, M. J., Collins, B., and Ridgway, S. T., "Theoretical Limits on Extrasolar Terrestrial Planet Detection with Coronagraphs," *The Astrophysical Journal* **167**, 81–99 (Nov. 2006).
3. Trauger, J. T. and Traub, W. A., "A laboratory demonstration of the capability to image an Earth-like extrasolar planet," *Nature* **446**, 771–773 (Apr. 2007).
4. Cavarroc, C., Boccaletti, A., Baudoz, P., Fusco, T., and Rouan, D., "Fundamental limitations on Earth-like planet detection with extremely large telescopes," *Astronomy and Astrophysics* **447**, 397–403 (Feb. 2006).
5. Baba, N. and Murakami, N., "A Method to Image Extrasolar Planets with Polarized Light," *The Publications of the Astronomical Society of the Pacific* **115**, 1363–1366 (Dec. 2003).

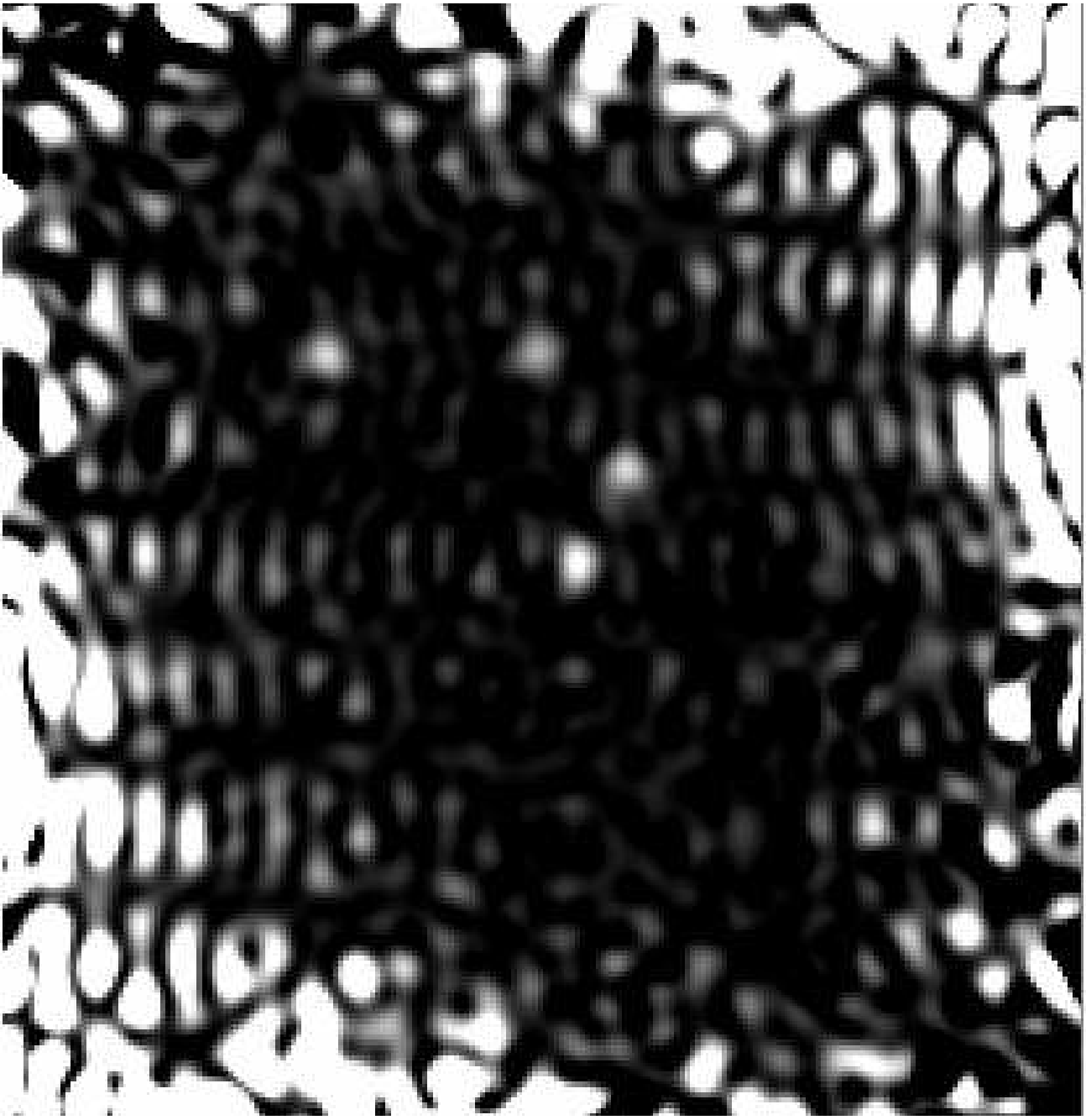

Figure 5. *SCC post-processed image of the last iteration image corresponding to a total exposure time of* $\sim 3\,hours$. 2.10^{-10} *companions are present at* 1, 3, 5 *and* $7\,\lambda_0/D$ *on a spiral. The field of view is about* $34 \times 34\,\lambda/D$. *The intensity scale is linear.*

6. Marois, C., Doyon, R., Nadeau, D., Racine, R., Riopel, M., Vallée, P., and Lafrenière, D., "TRIDENT: An Infrared Differential Imaging Camera Optimized for the Detection of Methanated Substellar Companions," *The Publications of the Astronomical Society of the Pacific* **117**, 745–756 (July 2005).
7. Guyon, O., "Imaging Faint Sources within a Speckle Halo with Synchronous Interferometric Speckle Subtraction," *The Astrophysical Journal* **615**, 562–572 (Nov. 2004).

8. Codona, J. L. and Angel, R., "Imaging Extrasolar Planets by Stellar Halo Suppression in Separately Corrected Color Bands," *The Astrophysical Journal* **604**, L117–L120 (Apr. 2004).
9. Baudoz, P., Boccaletti, A., Baudrand, J., and Rouan, D., "The Self-Coherent Camera: a new tool for planet detection," in [*IAU Colloq. 200: Direct Imaging of Exoplanets: Science Techniques*], Aime, C. and Vakili, F., eds., 553–558 (2006).
10. Galicher, R. and Baudoz, P., "Expected performance of a self-coherent camera," *Comptes Rendus Physique* **8**, 333–339 (Apr. 2007).
11. Galicher, R., Baudoz, P., and Rousset, G., "Wavefront error correction and Earth-like planet detection by Self-Coherent Camera in space," *Astronomy and Astrophysics* **-**, – (June submitted).
12. Bordé, P. J. and Traub, W. A., "High-Contrast Imaging from Space: Speckle Nulling in a Low-Aberration Regime," *The Astrophysical Journal* **638**, 488–498 (Feb. 2006).
13. Wynne, C. G., "Extending the bandwidth of speckle interferometry.," *Optics Communications* **28**, 21–25 (1979).